

Steady states of a driven dissipative dipolar XXZ chain

C D Parmee^{1,2,3}  and N R Cooper¹

¹ TCM Group, Cavendish Laboratory, University of Cambridge, JJ Thomson Avenue, Cambridge, CB3 0HE, United Kingdom

² Department of Physics, Lancaster University, Lancaster, LA1 4YB, United Kingdom

E-mail: c.parmee@lancaster.ac.uk

Received 29 January 2020, revised 23 March 2020

Accepted for publication 15 April 2020

Published 5 June 2020



Abstract

We study theoretically a driven dissipative one-dimensional XXZ spin-1/2 chain with dipole coupling and a tunable strength of the Ising and XY interaction. Within a mean-field approximation, we find a rich phase diagram with uniform, spin density wave, antiferromagnetic and oscillatory phases, as well as regions of phase bistability. We study the phase diagram of small quantum systems using exact diagonalisation, and compare the results to the mean-field theory. We find that while expectation values only capture the uniform phases of the mean-field theory, fluctuations about these expectation values give signatures of spatially non-uniform phases and bistabilities. We find these signatures for all ratios of the Ising to XY interaction, showing that they appear to be general features of spin-1/2 systems.


Keywords: open quantum systems, phase diagrams, dipole interactions, cold atoms, cold polar molecules, optical bistability

(Some figures may appear in colour only in the online journal)

1. Introduction

The study of quantum systems driven far from equilibrium has attracted much interest over the last few years. Although not as well understood as their equilibrium counterparts, non-equilibrium phenomena are in fact rather prevalent, as any experiment has some form of interaction with an environment, which will induce dissipative processes. Whereas these processes could be viewed as a nuisance, recent studies have shown that the interplay between an external drive and dissipation can produce exotic non-equilibrium phases such as spin density waves (SDW), antiferromagnetic phases (AFM), persistent long-time oscillations (OSC) and phase bistabilities within spin-1/2 systems [1–6] and higher spin systems [7]. Therefore, understanding the long-time steady state phases that can occur in open quantum systems is an intense area of current research.

³ Author to whom any correspondence should be addressed.

 Original content from this work may be used under the terms of the [Creative Commons Attribution 4.0 licence](https://creativecommons.org/licenses/by/4.0/). Any further distribution of this work must maintain attribution to the author(s) and the title of the work, journal citation and DOI.

In order to capture the steady state phases in a macroscopically large system, it is common to employ a mean-field approximation, where spatial correlations between sites are ignored. While the use of the mean-field approximation is well understood in equilibrium phenomena, an open question that still remains is the validity of the mean-field approximation for dissipative systems. For thermal gases in three-dimensions, one expects the mean-field approximation to become valid as quantum fluctuations become negligible [8, 9]. However, for cold systems and/or systems in reduced dimensions, where quantum fluctuations are more important, this is not necessarily the case. There have already been many studies into the true phases and transitions for the driven dissipative spin systems. These have involved exact diagonalisation and quantum Monte Carlo wavefunction approaches for small system sizes [10–13], or incorporating the use of Keldysh methods [14], cluster mean-field [15–18], Gutzwiller Monte Carlo approaches [19], corner-space renormalisation [20] or variational approaches [21] and matrix product and tensor network methods [22–27] to study larger systems. These studies have shown that first order transitions in the mean-field

approximation can become second order when quantum fluctuations are included, and that bistabilities can be lost. They have also shown that the emergence of certain phases, such as AFM or long-time oscillations may not occur in low dimensional spin-1/2 systems.

Despite the disagreements between mean-field and exact numerics of quantum systems, the mean-field approximation can still serve as an indicator of features that emerge in the full quantum system. For example, it has been shown that regions of mean-field bistability for the Ising model correspond to long spatial correlations in the full quantum model [28]. Also, while bistability has not been observed in finite-sized quantum spin systems, the bistable nature of the mean-field solutions is evident in quantum trajectories of the system [4, 10, 12, 13] and also results in a decrease in the spectral gap of the Liouvillian [4]. Therefore, it is interesting to ask how general these features are when comparing quantum results to those within the mean-field approximation, and if there are other consequences of the mean-field results for the full quantum dynamics.

In this paper, we study a driven-dissipative XXZ model with a tunable dipole-coupled XY and Ising interaction as a function of detuning and external drive strength. The tunable XY and Ising interaction connects the Ising model in reference [3] and the XY model in reference [4]. By calculating the nonequilibrium phase diagram at mean-field level, we find how the phases evolve as we move away from these two limits, finding the emergence of SDW, antiferromagnetism, temporal oscillations and bistabilities. We then analyse small quantum systems and carry out an in-depth comparison to our mean-field phase diagram. We find features in observables of the full quantum model which relate to mean-field bistabilities and spatial phases. The tunable Ising to XY interaction allows us to track these signatures with changes in the interaction, and shows that the quantum results are general features of spin models, and that the mean-field approximation still gives useful results in describing the full quantum dynamics.

The rest of this paper is organised as follows. In section 2, we describe the model, then in section 3, we derive the mean-field phase diagram. In section 4 we look at the full quantum model and then discuss the results and draw conclusions in section 5.

2. Model

The system consists of a large number, N , of atoms or polar molecules in a one-dimensional (1D) array. Two internal dipolar energy levels, $|g\rangle$ and $|e\rangle$, are isolated and the transition between them driven by an external drive detuned from resonance. The system can then be modelled as a spin-1/2 system, interacting via dipole-dipole interactions with a Rabi drive and detuning. The two-level transition also has a finite lifetime, comparable to the time scales of interaction, which results in decay from the excited state. Under the Born and Markov approximations, the dynamics of the system are described by the following master equation ($\hbar = 1$)

$$\frac{d\hat{\rho}(t)}{dt} = -i [\hat{H}, \hat{\rho}(t)] + \frac{\Gamma}{2} \sum_i^N [2\hat{\sigma}_i^- \hat{\rho}(t) \hat{\sigma}_i^+ - \{\hat{\sigma}_i^+ \hat{\sigma}_i^-, \hat{\rho}(t)\}], \quad (1)$$

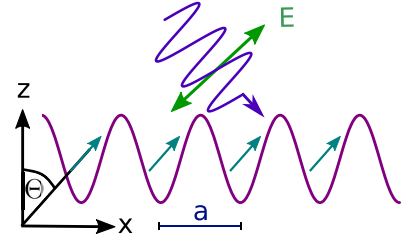


Figure 1. A schematic of a 1D array of atoms or polar molecules under an external drive. The electric field, shown by the green arrow, is oriented at an angle Θ to the z axis and controls the orientation of the dipoles. The lattice spacing is denoted by a .

where the spin operators are defined as $\hat{\sigma}_i^z = |e_i\rangle\langle e_i| - |g_i\rangle\langle g_i|$, $\hat{\sigma}_i^- = |g_i\rangle\langle e_i|$ and $\hat{\sigma}_i^+ = |e_i\rangle\langle g_i|$, with $|e_i\rangle$ and $|g_i\rangle$ being the excited and ground states of the two-level system, respectively, on site i . The decay constant, Γ , is controlled by optical pumping [2], where the two level system is off-resonantly dressed by a third energy level. The effective decay constant of the two-level transition is then a combination of the decay rate of the original two-level system and the decay rate of the third energy level. This allows us to tune the decay independently from the interaction between the two-level systems. The Hamiltonian is given by

$$\hat{H} = \frac{\Omega}{2} \sum_i^N \hat{\sigma}_i^x - \frac{\Delta}{2} \sum_i^N \hat{\sigma}_i^z + \sum_{i \neq j}^N \frac{J}{4R_{ij}^3} \times [\cos \alpha \hat{\sigma}_i^z \hat{\sigma}_j^z + \sin \alpha (\hat{\sigma}_i^y \hat{\sigma}_j^y + \hat{\sigma}_i^x \hat{\sigma}_j^x)], \quad (2)$$

where $R_{ij} = |r_i - r_j|$, with r_i being the position vector of a two-level system at site i , and $\hat{\sigma}_i^x = |e_i\rangle\langle g_i| + |g_i\rangle\langle e_i|$ and $\hat{\sigma}_i^y = i|g_i\rangle\langle e_i| - i|e_i\rangle\langle g_i|$. The detuning is given by $\Delta = \omega_d - \omega_{eg}$, with ω_d being the drive frequency and ω_{eg} the two-level transition frequency, and the drive strength is given by the Rabi coupling Ω . We note that the power law coupling is motivated by experiment but is not crucial for the results presented here, i.e. a nearest-neighbour coupling would also work. The dipole-dipole interaction is given by $J = J_0 a^3 (1 - 3 \sin^2 \Theta)$ where a is the lattice spacing (see figure 1) and the parameter J_0 is given by $J_0 = |\mathbf{d}|^2 / 4\pi\epsilon_0 a^3$.

The angle Θ is the orientation of the dipoles, and can be tuned by application of a dc electric field. The parameter α relates the relative strength of the Ising and XY dipole interactions and can take values between $-\pi$ to π . However, we only focus on the range $0 \leq \alpha < \pi$ as values below zero simply correspond to a change in the sign of J . Tuning the value of α depends on the choice of internal states and external fields, with $\cos \alpha$ being related to the difference in dipole moments of the groundstate and excited state, and $\sin \alpha$ being related to the transition dipole moment between the groundstate and excited state [29, 30].

For the remainder of the paper, we work with $\Theta = \pi/2$. Other values of Θ will result in a sign change and scaling of the interaction in 1D, but will not lead to significant changes in the types of phases that appear in our system, only in the size of the regions as a function of Δ and Ω . Also, we will only study $0 \leq \alpha < \pi$, as the values $-\pi \leq \alpha < 0$ will result in the same

phases as for $0 \leq \alpha < \pi$ but with the phase diagram reflected about $\Delta = 0$ due to the sign change in the interaction term. Therefore, it is sufficient to consider the range $0 \leq \alpha < \pi$ and $\Theta = \pi/2$ to cover all phases that can occur in the 1D system. Finally, we choose a value of $J_0 a^3 / \Gamma = 5$ for the rest of this paper. We should find similar results for other nearby values of $J_0 a^3 / \Gamma$, but expect that for $J_0 a^3 / \Gamma \ll 1$, we will only find spatially uniform phases in the system as the spins become effectively decoupled.

In order to find the long-time steady state of equation (1), we make a Gutzwiller mean-field approximation which results in taking $\hat{\rho}(t) = \otimes \hat{\rho}_i(t)$, where $\hat{\rho}_i(t)$ is a density matrix on site i , and we effectively ignore correlations between spins. Then, by taking the trace of equation (1) over all the sites except a given site j , we obtain the equations of motion as

$$\begin{aligned} \frac{dS_j^x}{dt} &= -\Gamma S_j^x - \Delta S_j^y + 2 \sin \alpha \sum_{i(\neq j)}^N \frac{J}{R_{ij}^3} S_i^z S_j^y \\ &\quad - 2 \cos \alpha \sum_{i(\neq j)}^N \frac{J}{R_{ij}^3} S_i^z S_j^x, \\ \frac{dS_j^y}{dt} &= -\Gamma S_j^y - \Omega S_j^z + \Delta S_j^x - 2 \sin \alpha \sum_{i(\neq j)}^N \frac{J}{R_{ij}^3} S_i^z S_j^x \\ &\quad + 2 \cos \alpha \sum_{i(\neq j)}^N \frac{J}{R_{ij}^3} S_i^z S_j^y, \\ \frac{dS_j^z}{dt} &= -\Gamma \left(S_j^z + \frac{1}{2} \right) + \Omega S_j^y - 2 \sin \alpha \sum_{i(\neq j)}^N \frac{J}{R_{ij}^3} (S_i^y S_j^x - S_j^y S_i^x), \end{aligned} \quad (3)$$

where $S_j^\beta = \frac{1}{2} \text{Tr}\{\hat{\sigma}_j^\beta \hat{\rho}(t)\}$ are the spin expectation values. The Rabi term in the Hamiltonian, equation (2), drives transitions between the excited and ground state of the two-level systems, causing the spins to try to align along the S^x axis, resulting in driving of the S^z and S^y spin components in equation (3). Likewise, the detuning term in equation (2) shifts the energy of the two-level system, which drives the S^y and S^x spin components as the spins try to align along the S^z axis. To find the steady state solutions, we solve the dynamics of the non-linear equation (3) by evolving them into the long-time limit.

3. Mean-field phase diagram

We compute the mean-field phase diagram by finding the steady states of equation (3). To do this, we first employ a bipartite sublattice ansatz where we reduce the system to two independent sites repeating periodically throughout the lattice. This allows us to find the uniform and antiferromagnetic steady state solutions steady states of equation (3) without having to evolve the equations in time. Depending on the parameters, there can be up to three uniform solutions and three sets of antiferromagnetic solutions. To determine the final phases that exist in the system, we perform linear stability analysis of the resultant solutions to fluctuations with wave vectors

$ka = \pi m / N$, where N is the number of sites on the lattice and m is an integer in the range $0 \leq m \leq N$. In cases where the wave vector of instability is not equal to 0 or π , we expect spin density wave solutions to form and for the bipartite sublattice ansatz to fail. To confirm the sublattice ansatz results are correct, we solve the full dynamics of equation (3) by evolving the equations in time until the long-time limit (up to $t\Gamma = 200$) for a system size of $N = 100$ with periodic boundary conditions. Simulating the full dynamics also allows us to find the resultant phases in regimes where the sublattice ansatz breaks down. For our dynamical simulations, as an initial condition, we use either $(S^x, S^y, S^z) = (0, 0, -1/2)$ or, if examining phase instability, the steady state that becomes unstable.

In figure 2, we show a collection of phase diagrams as a function of Δ and Ω for select values of α in the range $0 \leq \alpha < \pi$. We find our phase diagrams for $\alpha = 0$ and $\alpha = \pi/2$ are similar to those for a nearest-neighbour Ising and XY model studied in references [3] and [4], respectively, indicating that the power-law nature of the dipole interactions has little influence over the steady states. The phase diagrams for other α values show how these phases change as we move away from the Ising and XY model limits. For all, or almost all, α values, we can see some general features that occur. Specifically, we can classify four key phases that emerge in the system. Firstly, for all α , there are the spatially uniform phases, which are shown by the white regions in the phase diagrams. At low Rabi drive, the uniform phase has a high spin magnitude and the spins close to the state with $S^z \approx -1/2$. We define this uniform phase as the U_1 phase. At high drive, the spatially uniform phase has a decreasing spin magnitude, with $S^z \approx 0$ and with $S^{x/y} \rightarrow 0$ for increasing Rabi drive, where the steady state density matrix of the system becomes proportional to the identity matrix [10]. We denote this as the U_2 phase. Both uniform phases occur for any spin half system even without interactions as they are just general solutions to the optical Bloch equations. For $\alpha = \pi/4$, we have a Heisenberg Hamiltonian which conserves total spin and results in only uniform phases. For all α , the U_1 phase smoothly crosses over into the U_2 phase for most parameter ranges. However, for $\alpha \neq \pi/4$, when the drive and detuning are comparable to the interaction strength ($J/\Gamma = -5$), regimes of bistability between the U_1 and U_2 exist, which lead to sharp transitions between the two phases. Which phase the system ends up in within this region depends on the initial conditions. These regions of bistability are denoted by the dark blue regions in the phase diagram.

It is also the case that when the drive and detuning are comparable to the interactions, for all $\alpha \neq \pi/4$, the uniform phases can become unstable to fluctuations, breaking translational invariance and giving rise to non-trivial phases. In the red regions, the uniform phase becomes unstable to fluctuations with a wavevector of $ka = \pi$ and a stable set of antiferromagnetic solutions exist. This results in the emergence of a canted AFM solution, with the nature of the AFM phases depending on the α value. The spin components for the AFM solutions have large deviations between the S^z components on alternate sites when $0 < \alpha < \pi/4$, and large deviations on alternate sites for both the S^x and S^z components when $3\pi/4 < \alpha < \pi$. However, when the XY interaction dominates, the AFM

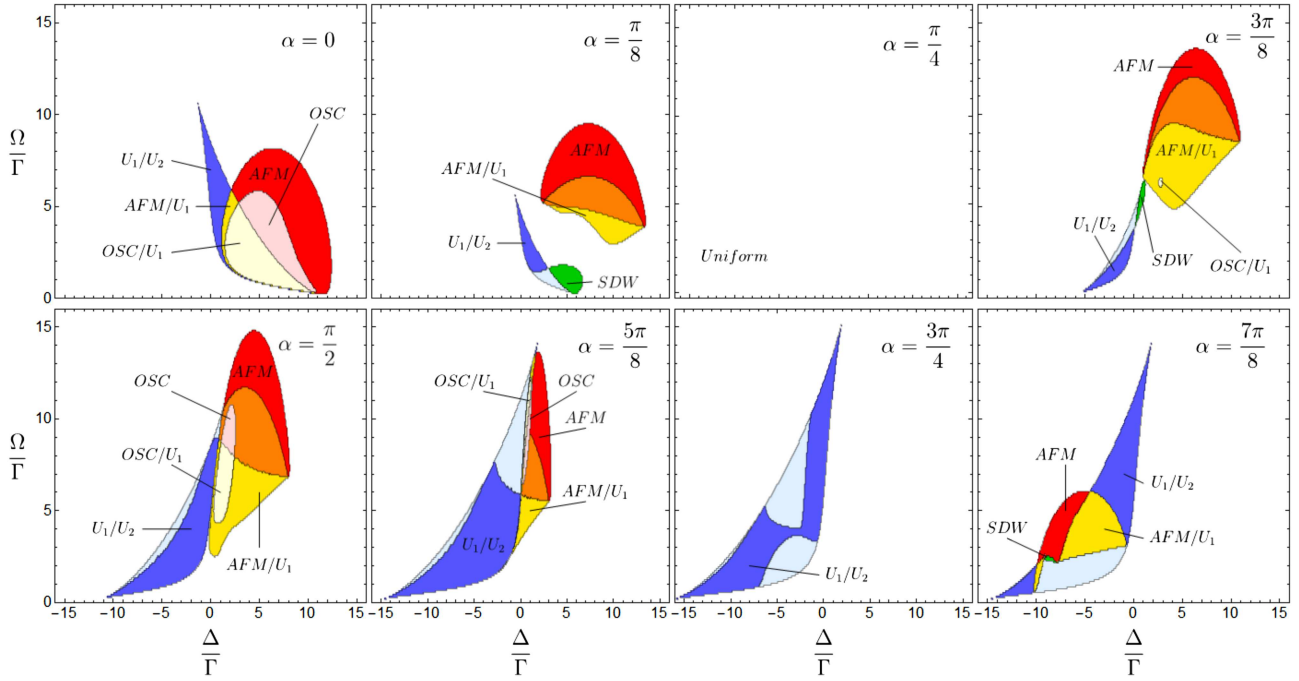


Figure 2. Phase diagrams as a function of Rabi coupling and detuning, for values of $0 \leq \alpha < \pi$ for a system with $J/\Gamma = -5$. We find the emergence of four key phases: uniform phases, spin density wave phases, antiferromagnetic phases and oscillatory phases. We also find examples of where these phases can be bistable with one another which means both phases can coexist within the corresponding parameter regime, and which phase the system ends up in depends on the initial conditions. These regions are denoted with double labelling e.g. AFM/ U_1 .

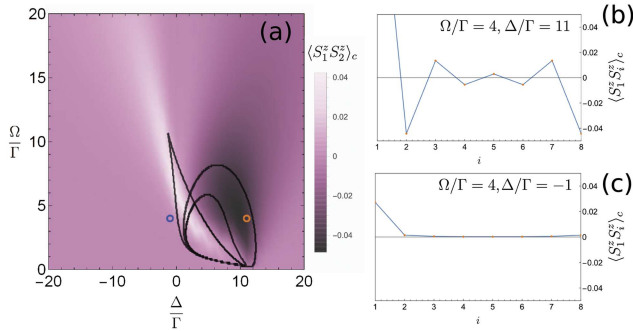


Figure 3. Examples of connected correlators for the quantum system with $J/\Gamma = -5$. (a) The $\langle \hat{S}_1^x \hat{S}_2^x \rangle_c$ connected correlator for $\alpha = 0$. The connected correlator becomes negative for nearest-neighbour sites when in the mean-field AFM region. The insets (b) and (c) show examples of how the connected correlator varies across sites for the orange and blue circle, respectively. We see that in both cases, long-range order is lost, but the changes of sign are as expected.

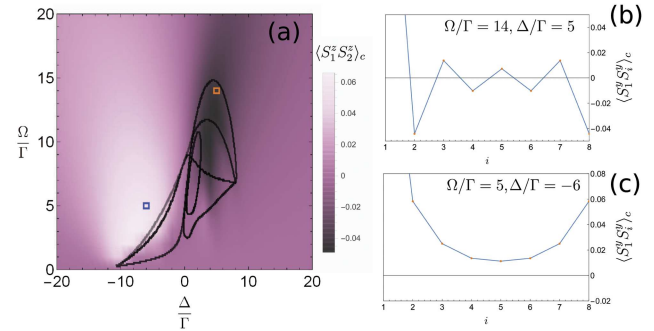


Figure 4. Examples of connected correlators for the quantum system with $J/\Gamma = -5$. (a) The $\langle \hat{S}_1^y \hat{S}_2^y \rangle_c$ connected correlator for $\alpha = \pi/2$. Again, the connected correlator changes sign between nearest-neighbours when in the mean-field AFM region. The insets (b) and (c) show examples of how the connected correlator varies across sites for the orange and blue squares, respectively.

solution has the strongest deviation in the S^y components between alternate sites. As well as instabilities to $ka = \pi$, the uniform phases can become unstable to $ka < \pi$ which results in the emergence of a spin density wave (SDW) phase. In the SDW phase, shown by the green regions, the spin orientation varies periodically through the lattice with a period set by the instability wavevector, ka . We find that there are no SDW instabilities for $\alpha = 0$. Therefore, it seems that SDW instabilities are related to presence of the XY interaction. The final key phase to emerge are persistent long-time oscillations, denoted by OSC, where the effects of the drive and interactions

dominate over the effects from dissipation. We find that all the oscillations emerge from the instability of the AFM phase, which undergoes a Hopf bifurcation, and inherit an AFM nature. The oscillations occur in the pink regions of the phase diagrams.

In several regions of the phase diagrams, multiple solutions to equation (3) coexist, which can lead to bistabilities. In the yellow regions, a stable uniform solution and stable set of AFM solutions exist, which results in AFM/ U_1 bistability. Similarly, in the light yellow regions, there is an OSC phase which is also bistable to the U_1 phase. We do find that there are cases where the oscillations become unstable

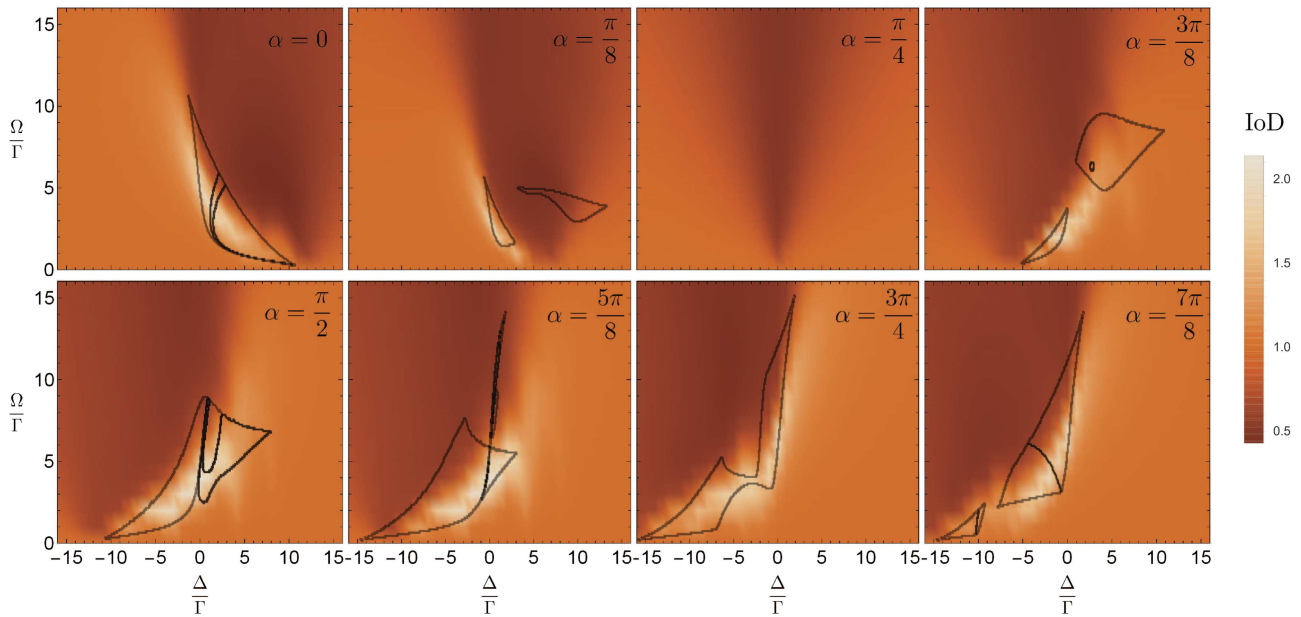


Figure 5. Index of dispersion (IoD) of the total number of excitations, $\sum_i^N (\hat{S}_i^z + \hat{1}/2)$ for a system with $J/\Gamma = -5$. We see there is an increase in the IOD in regions of bistability, before it drops quickly to $1/2$ when entering the region of the U_2 phase. The black contours show the regions of our mean-field phase diagram where bistability occurs.

and so only the uniform phase exists, which we have not marked in our phase diagram. In the light blue regions, both the U_1 phase and U_2 phase exist, but one becomes unstable to fluctuations. When simulating the dynamics in these regions, we find there is predominantly only one stable uniform solution, but also small regions of phase bistability between a SDW and uniform phase, which are not marked on the phase diagram. Similarly, in the orange regions, there exists both a uniform phase and an antiferromagnetic phase, but the uniform phase is unstable. We find when simulating the dynamics in this region that a spatial mixture of AFM and uniform phase appears in which regions of AFM phase are disrupted by a few sites of uniform phase. The degree of disruption to the AFM phase depends on the initial conditions.

4. Quantum phase diagram

Having now calculated the phase diagram at mean-field level, we now examine how it compares to the phase diagram of the full quantum system. To do this, we look at the steady state of small quantum systems with $N = 8$ spins and periodic boundary conditions. Despite the small system size, some distinct features emerge for the quantum system that reflect the mean-field phases.

We first examine the spin expectation values on each site for a direct comparison to the mean-field results. We find that for the quantum system, the expectation values on each site are uniform, with no spatial variation, for all values of detuning and drive. This is expected as the system is translationally invariant and spontaneous symmetry cannot be broken in finite-sized quantum systems. Therefore, the quantum expectation values must remain uniform. However, non-uniform phases will emerge within the

mean-field approximation, as the wave vectors that cause instability of the uniform phases, such as $ka = \pi$, are permitted. If we compare the quantum expectation values to the mean-field expectation values from our phase diagrams in the regions where stable uniform phases exist, we find there is good agreement when the magnitude of the Rabi drive and detuning are large, for all α . The difference between the expectation values becomes larger in regions where there is U_1/U_2 bistability. This is because we find no bistability in small quantum systems, but a smooth crossover between the U_1 and U_2 phases. Therefore the quantum expectation values will eventually differ from either choice of the U_1 or U_2 mean-field solution. For $\alpha = \pi/4$, we find the quantum and mean-field expectation values are equal to one another for all detuning and Rabi drive, which is due to the Heisenberg symmetry.

Although the expectation values only show a single uniform phase, the connected correlators between sites give insight into spatial structure of the fluctuations about the expectation values and possible emergence of non-uniform phases in large systems. In figure 3(a), we plot the connected correlator, $\langle \hat{S}_i^z \hat{S}_j^z \rangle_c = \langle \hat{S}_i^z \hat{S}_j^z \rangle - \langle \hat{S}_i^z \rangle \langle \hat{S}_j^z \rangle$, between a site i and its nearest-neighbour for $\alpha = 0$. We find that the connected correlator changes sign between nearest-neighbour sites in the region where AFM solutions exist in the mean-field, but maintains the same sign when in the uniform region. Figures 3(b) and (c) show examples of how the connected correlator varies across the lattice sites for a choice of Δ and Ω in the AFM region and in the uniform region, shown by the orange and blue circles, respectively. Both connected correlators lose long-range order quickly, but maintain an alternating sign in the AFM region, while being persistently positive in the uniform region. We also plot the $\langle \hat{S}_i^y \hat{S}_j^y \rangle_c$ connected correlator for $\alpha = \pi/2$ in

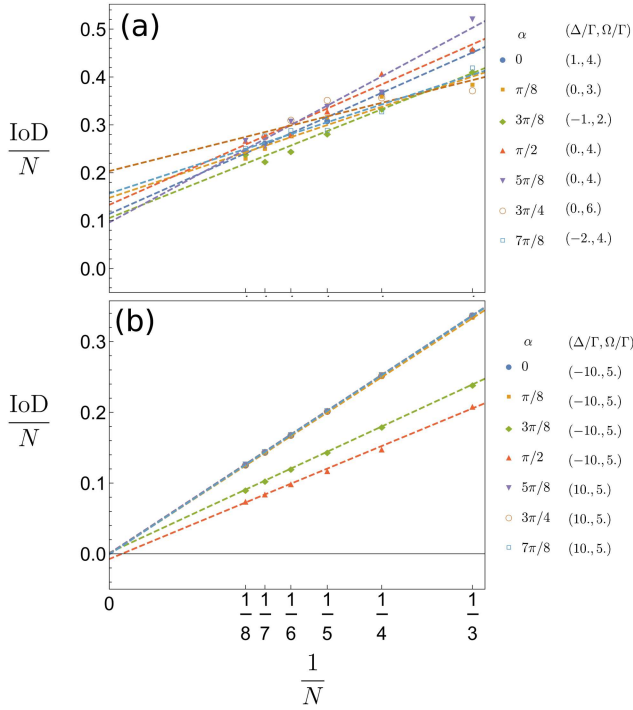


Figure 6. Scaling of the IoD with system sizes $N = 3$ to $N = 8$. The values of Δ/Γ and Ω/Γ used for each α value are listed by the side of the figure, and $J/\Gamma = -5$. (a) Scaling of the IoD for the point where the maximum IoD value at $N = 8$ occurs for each α except $\alpha = \pi/4$ where the $\text{IoD} \leq 1$. In all cases, the maximum of the IoD occurs near or within the bistable region of mean-field theory. We can see a clear trend that as we scale the data with N , there is a non-zero intercept at the infinite lattice limit, which agrees with the semi-classical behaviour of the IoD given in equation (5). (b) Scaling of the IoD for a point well outside the bistability region. The intercept now drops to zero, which again agrees with the semi-classical behaviour of the IoD.

figure 4, finding again a loss of long-range order, but sign changes between nearest-neighbour sites in the region where AFM solutions exist in the mean-field phase diagram. The connected correlator plots for $\alpha = 0$ and $\alpha = \pi/2$ are similar to those in references [3] and [4], respectively. For both figures 3 and 4, the choice of connected correlator is based on the spin component with the strongest deviation from the spatially uniform phase in the mean-field analysis.

We find the behaviour of the quantum model that is best described by the mean-field theory is found when studying the quantum dynamics in the regions of mean-field phase bistability. In regions of bistability, many studies [4, 10, 12] have found examples of bimodality in the expectation value distributions when using quantum Monte Carlo wavefunction methods. This bimodality arises when there are two stable mean-field solutions where, in the mean-field limit, each steady state behaves as if the minimum of a double well potential. In the absence of fluctuations, the system will sit in either steady state indefinitely. However, in the full quantum system, fluctuations induce transitions between these steady states, giving a single expectation value, but leaving a double well structure in the expectation value distributions. Bistability brings the greatest change in S^z values between the two

mean-field phases, and so we study the total number of excitations, $\sum_i^N (\hat{S}_i^z + \hat{1}/2)$. In the quantum system, the expectation value of the total excitations will take an average of the two mean-field phases, and so it is not possible to detect bimodality in the underlying distribution by looking at the expectation values alone. However, bimodal behaviour in a distribution can instead be observed by studying the index of dispersion (IoD) of $\sum_i^N (\hat{S}_i^z + \hat{1}/2)$, which is given by

$$\text{IoD} = \frac{\sum_{i,j}^N \left(\langle \hat{S}_i^z \hat{S}_j^z \rangle - \langle \hat{S}_i^z \rangle \langle \hat{S}_j^z \rangle \right)}{\sum_i^N \left(\langle \hat{S}_i^z \rangle + 1/2 \right)}, \quad (4)$$

and is a measure of a distribution's variance normalised by its mean. In the limit of zero Rabi drive, when $\langle \hat{S}_i^z \rangle = -1/2$, we have $\text{IoD} = 1$, whereas in the limit of high Rabi drive, when $\langle \hat{S}_i^z \rangle \approx 0$, we have $\text{IoD} = 1/2$. Between these two limits, the IoD will either decrease or, when there is a bimodality in the distribution, increase above unity. In figure 5, we plot the IoD as a function of Δ and Ω . We can see from figure 5 that there are regions of enhanced fluctuations, which agree well with the bistability region for all α values, suggesting that the large peak in the IoD is indeed due to the double well structure of the mean-field solution appearing in the quantum steady state. Large peaks in the IoD were found for a nearest-neighbour XY model in reference [4], similar to our $\alpha = \pi/2$ case, but our results show that this IoD peak is in fact a general feature of spin systems.

We now analyse further how well the IoD behaviour is captured by fluctuations about two mean-field solutions. We assume that the system fluctuates between two steady states, with probability P_1 to occupy the mean-field uniform state with a spin z component S_1^z , and a probability $P_2 = 1 - P_1$ to occupy the mean-field uniform state with a spin z component of S_2^z . In this situation, the IoD is given by

$$\text{IoD}_{\text{Cl}} = \frac{NP_1P_2(S_1^z - S_2^z)^2}{P_1S_1^z + P_2S_2^z + 1/2} - \frac{P_1(S_1^z)^2 + P_2(S_2^z)^2 - 1/4}{P_1S_1^z + P_2S_2^z + 1/2}. \quad (5)$$

Outside the regime of bistability, we have $P_2 = 0$, so the classical IoD reduces to $\text{IoD}_{\text{Cl}} = 1/2 - S_1^z$, where we recover $\text{IoD}_{\text{Cl}} = 1$ and $\text{IoD}_{\text{Cl}} = 1/2$ corresponding to the low and high drive limiting cases, respectively. However, inside the bistability regime, the IoD should scale with the system size. Therefore, a signature that the quantum model exhibits tunnelling between two mean-field bistable solutions would be for IoD/N to remain non-zero in the thermodynamic limit. Our mean-field phase diagram shows that uniform bistability occurs between the U_1 phase with $S^z \approx -1/2$ and the U_2 phase with $S^z \approx 0$. If, as an example, we assume $P_1 \approx P_2$, this gives an IoD intercept of $\lim_{N \rightarrow \infty} \text{IoD}/N = 0.25$. However, it is possible that the probabilities to reside in either mean-field state will not be equal.

In figure 6(a), we plot IoD/N vs $1/N$ for the point where the IoD is largest for $N = 8$, which lies inside the bistability region, for each α . In figure 6(b), we plot a point outside the bistability region. We can clearly see how there is a non-zero intercept for the scaling inside the bistability region, whereas the intercept drops to zero outside this region for each α . In

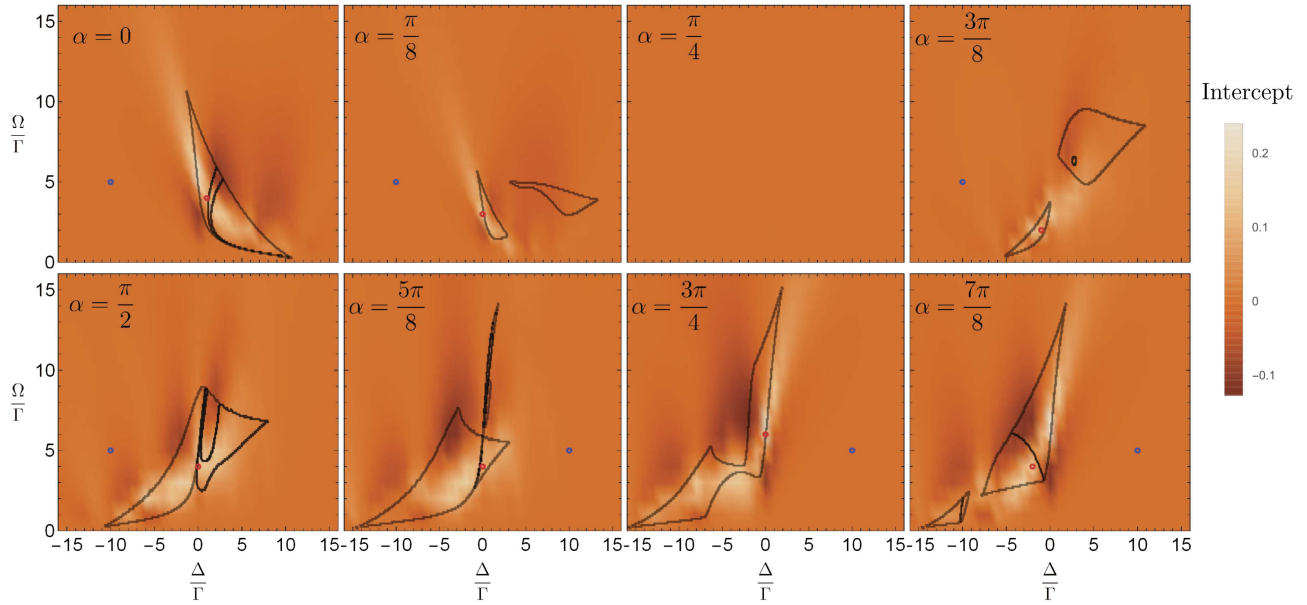


Figure 7. Plot of the linear fit intercept of IoD/N vs $1/N$ at each point of the phase diagram for a system with $J/\Gamma = -5$. Near and within the region of bistability, the intercept takes on a positive value, whereas it is typically zero elsewhere, although does become negative in places. For $\alpha = \pi/4$, the intercept is always 0 as there is no bistability. The occurrence of a positive finite value within the bistable region and zero value outside is expected from the semiclassical behaviour of the IoD given in equation (5). The red (light) and blue (dark) circles indicate the points shown in figures 6(a) and (b), respectively.

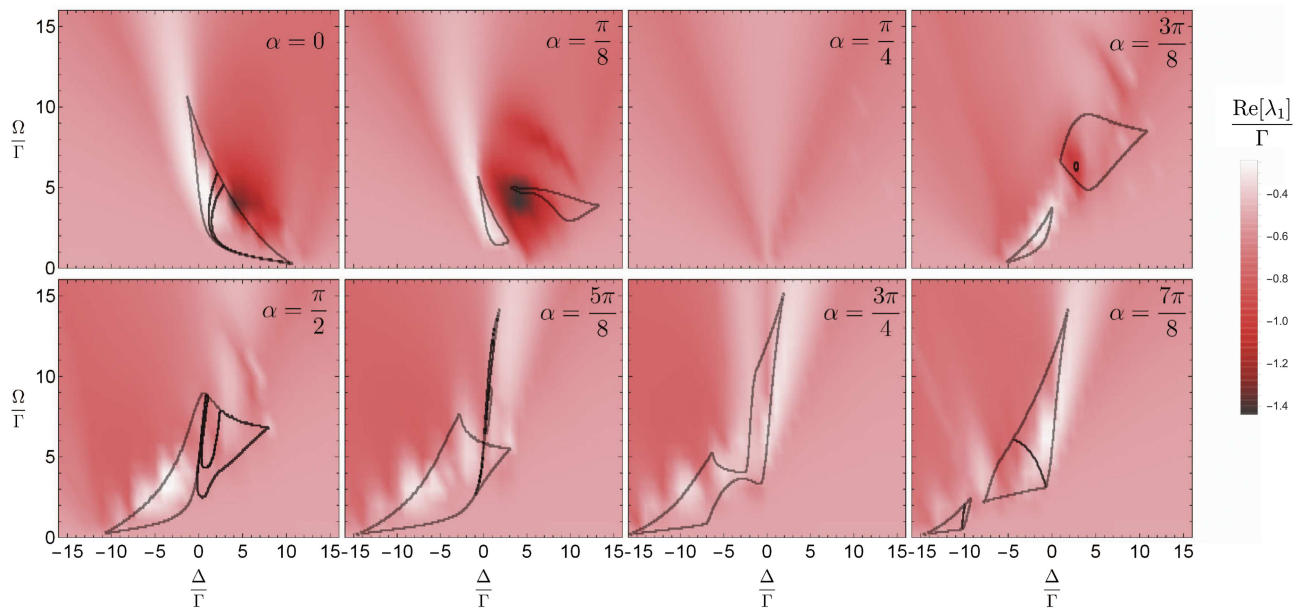


Figure 8. Real part of the spectral gap of the Liouvillian for a system with $J/\Gamma = -5$. We see that this is minimal within the regime of bistability for all α . The scaling of the spectral gap with system size is shown in figure 9.

figure 7, we apply the same linear scaling to each point in the phase diagram and plot the intercept. We find that the intercept takes positive non-zero values near and inside the region of bistability, but is typically zero elsewhere. The largest values of the intercept in the quantum model are typically of the order of the value ~ 0.25 expected from mean-field theory. There are also regions where the intercept becomes negative, which occur towards the edge or just outside the bistability region, which indicate a breakdown of the linear scaling at

large N as the IoD should always be positive. Overall, the presence of a positive finite value of IoD/N inside the bistable region indicates that the fluctuations in the quantum system are well described by fluctuations between two bistable mean-field solutions. For these system sizes, the fluctuations remain well-described by the mean-field theory, showing no evidence of vanishing in the thermodynamic limit. Eventually, for very large systems, described by the field theoretical method with local fluctuations [14], we expect that the IoD/N will tend to

zero except, perhaps, if there is a critical point at which the density matrix jumps discontinuously [31].

Bistability should also have consequences for the spectral gap of the Liouvillian. The master equation, equation (1), can be written as $d\hat{\rho}(t)/dt = \mathcal{L}\hat{\rho}(t)$, where \mathcal{L} is the Liouvillian superoperator that determines the evolution of the system. By expanding the density matrix in eigenvectors of the Liouvillian superoperator, we can write a generic quantum state as

$$\begin{aligned} \hat{\rho}(t) &= \exp(\mathcal{L}t)\hat{\rho}(0) \\ &= \hat{\rho}_{ss} + \sum_{i=1}^{4^N-1} \text{Tr}\{\hat{L}_i\hat{\rho}(0)\}\hat{R}_i e^{\lambda_i t}, \end{aligned} \quad (6)$$

where \hat{L}_i and \hat{R}_i are the left and right eigenvectors of \mathcal{L} , respectively, with complex eigenvalues, λ_i . The eigenvalues of the Liouvillian come in complex-conjugate pairs due to the Hermitian nature of the density matrix, with a negative real part corresponding to the decay of the eigenvalues and the imaginary part corresponding to coherences. We order the eigenvalues, λ_i , by the increasing magnitude of their real part. There is always at least one zero eigenvalue of the Liouvillian matrix ($\lambda_0 = 0$) corresponding to the steady state of the system, which we have extracted from the sum in equation (6) and denoted the eigenvector as $\hat{\rho}_{ss} \equiv \hat{R}_0$. Note that $\hat{\rho}_{ss}$ has unit trace and the remaining eigenvectors, \hat{R}_i , are traceless.

In systems with bistability, the spectral gap (i.e. the eigenvalue with smallest real part) should close so that the system has two steady states. For small quantum systems, the gap will remain non-zero [32]. It has also been shown that for large quantum systems, similar to the above model for $\alpha = \pi/2$, the closing of the gap should not to occur for three dimensions [14]. In essence, the non-zero spectral gap in these cases indicates that the quantum system can exhibit tunneling between the two mean-field minima, precluding bistability at times longer than the inverse spectral gap. Still, in view of the above results showing that the fluctuations in the quantum system are strongly affected by the mean-field bistability (with an IoD/N that is qualitatively described by a bistable mean-field theory even for large N), we would expect the region of mean-field bistability should also be reflected in the spectral gap. In figure 8, we plot the real part of the spectral gap [33] for the system with $N = 6$ spins. We see there is indeed a reduction in the gap size in the bistability region compared to elsewhere in the phase diagram.

Employing finite-size scaling, we examine how the real part of the spectral gap changes with increasing N . Figure 9 shows how the spectral gap changes for $N = 3$ to $N = 7$ for the same parameters used to examine the IoD in figure 6. For the parameters inside the mean-field bistability region, we find that the spectral gap decreases with larger system size, although there are large fluctuations in this behaviour for $\alpha = \pi/2$ and $\alpha = 5\pi/8$ which are likely finite-size effects. It appears that for all α , the gap will eventually saturate at higher system size rather than close. For the parameters outside the mean-field bistability region, the spectral gap only has small changes

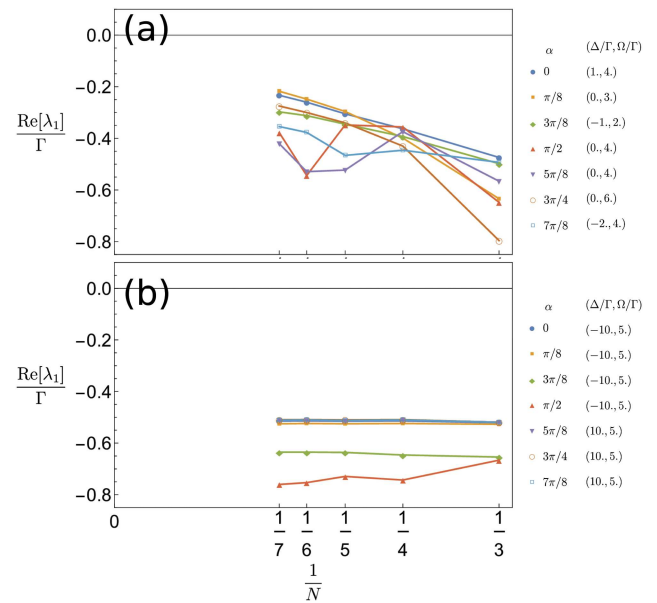


Figure 9. Scaling of the spectral with system size for systems of size $N = 3$ to $N = 7$. The values of Δ/Γ and Ω/Γ used for each α value are listed by the side of the figure, and $J/\Gamma = -5$. (a) Scaling of the spectral gap for the coordinates inside the mean-field bistability region examined figure 6(a). We can see that the gap minimum decreases for all α as N increases. For all α , we find that the minimum gap always lies within the region of mean-field bistability for $N > 3$ and that our finite-sized scaling indicates the gap may saturate in the infinite lattice limit. (b) Scaling of the spectral gap for coordinates outside the mean-field bistability region examined in figure 6(b). We see there is little change to the spectral gap, and in all cases, the gap remains below the natural linewidth, $\Gamma/2$, showing no tendency to decrease.

with increasing system size. For all α , the gap shows no tendency to decrease and remains below the natural linewidth, $\Gamma/2$. Overall, we find the largest decrease in spectral gap lies within the regions of uniform bistability, with little change in the gap outside this region. These results indicate that the gap does not close for large systems—i.e. there is no true bistability at long times—but do show that the mean-field results indicate regions in which the full quantum dynamics show a slow down on the approach to the steady state. As discussed above, these arrested dynamics are associated with a scaling of the IoD/N that appears to saturate at large N . While one cannot conclude that such a scaling will continue to infinite N , these results indicate that the mean-field results have significant influence in determining the behaviour of the quantum system for the accessible system sizes. There is the possibility that a critical point where the gap eventually closes will emerge somewhere within the bistability region, leading to a first order transition [31]. Our results for gap scaling at other points in the bistability region show no evidence of this for $N = 3$ to $N = 6$. However, this could be because we are restricted to small system sizes and the gap may close for large enough systems.

To measure the spectral gap in experiment, one could look at two-time correlators, whose decay depends specifically on the spectral gap in the long-time limit. For two operators, \hat{A} and \hat{B} , the two-time correlator is given by [34]

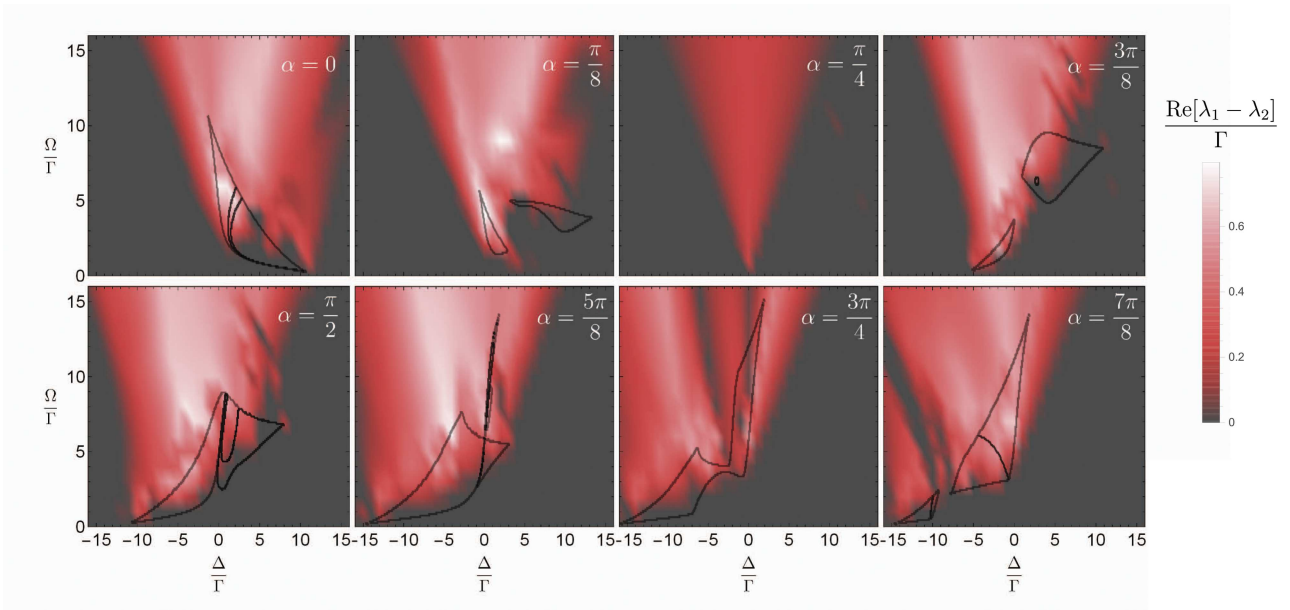


Figure 10. Difference between the real part of the spectral gap and the real part of the next eigenvalue in the spectrum for a system with $J/\Gamma = -5$. We see for a dominant Ising interaction, there is an increase in separation which indicates the spectral gap could be measured from the decay of the two-time correlator. For an XY dominated interaction, the difference between the real part of the eigenvalues is much smaller and so measuring the gap from the two-time correlator will be harder.

$$\begin{aligned}
 \langle \hat{A}(t + \tau)\hat{B}(t) \rangle &= \text{Tr}\left\{ \hat{A}e^{(\tau+t-t)\mathcal{L}}\hat{B}\hat{\rho}(t) \right\} \\
 &= \text{Tr}\left\{ \hat{B}\hat{\rho}(t) \right\} \text{Tr}\left\{ \hat{A}\hat{\rho}_{ss} \right\} + \sum_{i=1}^{4^N-1} e^{\lambda_i\tau} \\
 &\quad \times \text{Tr}\left\{ \hat{L}_i\hat{B}\hat{\rho}(t) \right\} \text{Tr}\left\{ \hat{A}\hat{R}_i \right\}, \quad (7)
 \end{aligned}$$

where we have inserted the density matrix expansion given in equation (6). If we allow $t \rightarrow \infty$ so we study the two-time correlator in the steady state, then equation (7) simplifies to

$$\begin{aligned}
 \lim_{t \rightarrow \infty} \langle \hat{A}(t + \tau)\hat{B}(t) \rangle &= \text{Tr}\left\{ \hat{A}\hat{\rho}_{ss} \right\} \text{Tr}\left\{ \hat{B}\hat{\rho}_{ss} \right\} \\
 &\quad + \sum_{i=1}^{4^N-1} \text{Tr}\left\{ \hat{L}_i\hat{B}\hat{\rho}_{ss} \right\} \text{Tr}\left\{ \hat{A}\hat{R}_i \right\} e^{\lambda_i\tau} \\
 &\approx \text{Tr}\left\{ \hat{A}\hat{\rho}_{ss} \right\} \text{Tr}\left\{ \hat{B}\hat{\rho}_{ss} \right\} \\
 &\quad + \text{Tr}\left\{ \hat{L}_1\hat{B}\hat{\rho}_{ss} \right\} \text{Tr}\left\{ \hat{A}\hat{R}_1 \right\} e^{\lambda_1\tau}, \quad (8)
 \end{aligned}$$

where in the last line we have assumed that τ is large and that the spectral gap, λ_1 , is well separated from the rest of the Liouvillian spectrum. This shows how the two-time correlator will decay exponentially with a decay time set by the spectral gap. Therefore, if the spectral gap does decrease in a given parameter regime, we should find that any two-time correlator will have a much longer temporal decay than in regions where the spectral gap is large. In figure 10, we plot the difference in real part of the first and second eigenvalues of the Liouvillian to see if the spectral gap is well separated from the spectral bulk. We find for a dominant Ising interaction, there is a separation

inside the bistable regime, so measuring the gap from the connected correlator decay should be possible. For a dominant XY interaction, the gap from the bulk is quite small and therefore measuring the gap from the two-time correlator will be harder.

5. Discussion and conclusions

We have studied the mean-field phase diagram of an driven-dissipative XXZ model with a tunable XY and Ising interaction, finding that the interplay between drive and dissipation leads to four key types of non-equilibrium phases. Specifically, we find uniform phases, AFM phases, SDW phases and OSC phases, as well as bistabilities between these phases, and have studied how these phases change with the tuning of the Ising to XY interaction. Such a system could be readily studied with Rydberg atoms [35], trapped ions [36] or polar molecules [29, 37], where dissipation can be controllably induced with optical pumping [2].

Our in-depth study of the full quantum system for a small number of spins shows that the expectation values of the small quantum system agree well with the mean-field uniform phases at strong Rabi drive and detuning, but do not agree as well when the drive and detuning are comparable to the interaction strength. The biggest difference between the mean-field and quantum results is the small quantum system does not exhibit any bistabilities, OSC, AFM or SDW phases. The fact that only uniform phases occur for the small quantum system is expected as the system is translationally invariant and symmetry cannot be spontaneously broken for finite sized systems without a closing of the spectral gap of the Liouvillian. This closing of the spectral gap does occur within the mean-field approximation, which is why we obtain non-uniform phases

there. However, for the quantum system, analysis of connected correlators shows how fluctuations about the expectation values give signatures of the non-spatially uniform mean-field phases and indicate the possibility that fluctuations could produce non-spatially uniform phases for large enough quantum systems. The strongest signatures of the mean-field can be found when looking at the behaviour of the quantum dynamics in regions of mean-field bistability, where study of the IoD of excitations shows enhanced fluctuations due to tunnelling between two mean-field states. Finally, we have shown a good agreement between the bistability region and a decrease in the real part of the spectral gap in the Liouvillian, which should be observable by a increase in the decay times of two-time correlators. The decrease in spectral gap and enhanced fluctuations could also lead to observable metastable behaviour between the two mean-field states even for finite-sized systems.

We have found that our results for $\alpha = 0$ and $\alpha = \pi/2$ agree with similar studies with nearest-neighbour interactions [3, 4], both at the mean-field and quantum level, indicating that the $1/r^3$ power-law nature of the interactions have little effect on the resultant phases. Given this and the fact that our system is 1D, modelling the system with DMRG [38] to achieve larger system sizes should be possible. It would be interesting to see if larger systems show evidence of breaking of spatial uniformity we have seen in our mean-field analysis. While we do not expect true long-range order, the mean-field theory could still be apparent in local correlations. As we have explained, true bistability is not found in the quantum model, as evidenced by a spectral gap that shows evidence of saturation at the largest N that we have studied. Still this gap is much suppressed compared to regions outside of the bistability, indicating a slow-down of the dynamics that is closely correlated with the regime of mean-field bistability. Also, we have shown that, even for the largest systems, the IoD scales linearly with system size within the region of bistability and has IoD/N taking a non-zero value in the large N limit. This is consistent with the existence of a quantum state that is formed by fluctuations between two mean-field states, even for this one-dimensional model. It would, of course, be interesting to extend these studies to see how the results evolve for even larger systems, for example, causing IoD/N to tend to zero, except possibly at a critical point where the gap closes. Looking at how the IoD and spectral gap behaves in higher dimensionalities would also be interesting as the mean-field is expected to become more valid with increasing coordination number.

6. Notes

Statement of compliance with EPSRC policy framework on research data: all data accompanying this publication are directly available within the publication.

Acknowledgments

This work was supported by EPSRC Grant Nos. EP/K030094/1 and EP/P009565/1 and by the Simons Foundation.

ORCID iDs

C D Parmee  <https://orcid.org/0000-0002-8514-3785>

References

- [1] Chan C-K, Lee T E and Gopalakrishnan S 2015 *Phys. Rev. A* **91** 051601(R)
- [2] Lee T E, Gopalakrishnan S and Lukin M D 2013 *Phys. Rev. Lett.* **110** 257204
- [3] Lee T E, Häffner H and Cross M C 2011 *Phys. Rev. A* **84** 031402(R)
- [4] Wilson R M, Mahmud K W, Hu A, Gorshkov A V, Hafezi M and Foss-Feig M 2016 *Phys. Rev. A* **94** 033801
- [5] Qian J, Zhang L, Zhai J and Zhang W 2015 *Phys. Rev. A* **92** 063407
- [6] Parmee C D and Cooper N R 2018 *Phys. Rev. A* **97** 053616
- [7] Qian J, Dong G, Zhou L and Zhang W 2012 *Phys. Rev. A* **85** 065401
- [8] Carr C, Ritter R, Wade C G, Adams C S and Weatherill K J 2013 *Phys. Rev. Lett.* **111** 113901
- [9] Šibalić N, Wade C G, Adams C S, Weatherill K J and Pohl T 2016 *Phys. Rev. A* **94** 011401(R)
- [10] Olmos B, Yu D and Lesanovsky I 2014 *Phys. Rev. A* **89** 023616
- [11] Rota R, Minganti F, Biella A and Ciuti C 2018 *New J. Phys.* **20** 045003
- [12] Lee T E, Häffner H and Cross M C 2012 *Phys. Rev. Lett.* **108** 023602
- [13] Ates C, Olmos B, Garrahan J P and Lesanovsky I 2012 *Phys. Rev. A* **85** 043620
- [14] Maghrebi M F and Gorshkov A V 2016 *Phys. Rev. B* **93** 014307
- [15] Jin J, Biella A, Viyuela O, Mazza L, Keeling J, Fazio R and Rossini D 2016 *Phys. Rev. X* **6** 031011
- [16] Jin J, Biella A, Viyuela O, Ciuti C, Fazio R and Rossini D 2018 *Phys. Rev. B* **98** 241108(R)
- [17] Owen E T, Jin J, Rossini D, Fazio R and Hartmann M J 2018 *New J. Phys.* **20** 045004
- [18] Biella A, Jin J, Viyuela O, Ciuti C, Fazio R and Rossini D 2018 *Phys. Rev. B* **97** 035103
- [19] Huybrechts D and Wouters M 2019 *Phys. Rev. A* **99** 043841
- [20] Rota R, Storme F, Bartolo N, Fazio R and Ciuti C 2017 *Phys. Rev. B* **95** 134431
- [21] Weimer H 2015 *Phys. Rev. Lett.* **114** 040402
- [22] Cui J, Cirac J I and Bañuls M C 2015 *Phys. Rev. Lett.* **114** 220601
- [23] Mascarenhas E, Flayac H and Savona V 2015 *Phys. Rev. A* **92** 022116
- [24] Mendoza-Arenas J J, Clark S R, Felicetti S, Romero G, Solano E, Angelakis D G and Jaksch D 2016 *Phys. Rev. A* **93** 023821
- [25] Joshi C, Nissen F and Keeling J 2013 *Phys. Rev. A* **88** 063835
- [26] Kshetrimayum A, Weimer H and Orús R 2017 *Nat. Commun.* **8** 1291
- [27] Höning M, Muth D, Petrosyan D and Fleischhauer M 2013 *Phys. Rev. A* **87** 023401
- [28] Hu A, Lee T E and Clark C W 2013 *Phys. Rev. A* **88** 053627
- [29] Gorshkov A V, Manmana S R, Chen G, Demler E, Lukin M D and Rey A M 2011 *Phys. Rev. A* **84** 033619
- [30] Peter D 2015 Quantum states with topological properties via dipolar interactions *PhD Thesis* University of Stuttgart
- [31] Vicentini F, Minganti F, Rota R, Orso G and Ciuti C 2018 *Phys. Rev. A* **97** 013853
- [32] Schirmer S G and Wang X 2010 *Phys. Rev. A* **81** 062306
- [33] Navarrete-Benlloch C 2015 arXiv:1504.05266
- [34] Breuer H-P and Petruccione F 2007 *The Theory of Open Quantum Systems* (Oxford: Oxford University Press)
- [35] Glaetzle A W, Dalmonte M, Nath R, Gross C, Bloch I and Zoller P 2015 *Phys. Rev. Lett.* **114** 173002

- [36] Britton J W, Sawyer B C, Keith A C, Wang C-C J, Freericks J K, Uys H, Biercuk M J and Bollinger J J 2012 *Nature* **484** 489
- [37] Wall M L, Hazzard K R A and Rey A M 2015 *Mesoscale* vol 80309 (Singapore: World Scientific) pp 3–37
- [38] Schollwöck U 2005 *Rev. Mod. Phys.* **77** 259